ADVANCED MATERIALS

DOI: 10.1002/adma.200701673

On the Origin of the Color Shift in White-Emitting OLEDs**

By *Malte C. Gather*, *Ronald Alle*, *Heinrich Becker*, and *Klaus Meerholz**

Over the last decade the organic light-emitting diode (OLED) technology has been developed for the next generation of flat-panel displays. As the power efficiency of OLEDs has increased dramatically over the past years the focus of researchers in the field is now shifting towards lighting applications.[1,2] Inspired by the vision of large-area lighting panels providing ergonomic and economic anti-glare illumination, both industry and academia are in the process of developing efficient white light-emitting OLEDs (WOLEDs). However, in addition to the complications encountered in the field of flat-panel displays – such as device stability, cost of manufacturing, patternability, etc – lighting applications pose further challenges: First, the required brightness levels are usually considerably higher for lighting, which requires higher operating currents that can shorten the device lifetime. Second, the required power efficiencies are significantly higher in order to compete with established lighting technologies. Third, the size of the devices will be larger and the acceptable cost-per-area will be significantly lower. The simultaneous requirements of inexpensive material deposition and large area substrates renders solution-based approaches generally preferable compared to vacuum-based techniques. Finally, the WOLED must provide a stable and pure white electroluminescence (EL) spectrum, i.e. the light must be characterized by a high color-rending index (CRI) and the color-point has to remain stable – both over the entire operational lifetime of the device and for different brightness levels.

In the past, several groups claimed to have demonstrated devices that provide color-stable white emission.[3-6] However, most WOLEDs reported in the literature in fact show brightness-dependent color-shifts that significantly exceed the tolerable margin. This margin is typically defined as a CIE (Commision Internationale de l'Éclairage) coordinate change of 0.005 – 0.01 or less for both the x- and the y-value over orders of magnitude in brightness and over the entire operational lifetime.[7] Although different explanations for the notorious color-shift observed in most devices have been proposed there is still no consistent quantitative explanation.[8-11]

In this Communication we report on a detailed study of the brightness-dependent color-shift occurring in WOLEDs based on a white-emitting electroluminescent copolymer. We find that for this system neither saturation of the red-emitting chromophore nor a shift of the recombination/emission zone with increasing brightness are the dominant factors causing the color-shift.[12] Instead, we find that the shift in color with increasing brightness can be explained by the competition between electron trapping on the red-emitting chromophore sites and unperturbed charge transport through the organic layer. Furthermore, a quantitative model is derived which accurately describes the experimental data by comparing the transit time and the trapping rate for electrons. Based on these findings an optimized device with excellent color-stability has been developed.

Most solution-processed and many small molecule based WOLEDs currently discussed in the literature contain a single emissive layer which consists of a matrix material with a wide band-gap and one to three additional species emitting in different regions of the spectrum.[4,10,13,14] If the different components are blended together device stability can be an issue since phase separation may occur over time. One way to avoid this problem is to copolymerize the different components into a statistic copolymer.[11,15–17] In this work we followed a similar approach by using a white-emitting statistical copolymer (**PW**) consisting mainly of a wide band-gap poly-spirofluorene backbone (**BB**, 79 mol%) that has an electron mobility of 10^{-3} cm^2/Vs.[18] The other components are a hole-transporting unit (**HT**, 10 mol%), a blue-emitting chromophore (**BC**, 11 mol%), and small quantities of red- (**RC**, 0.04 mol%) and green- (**GC**, 0.05 mol%) emitting chromophores. To separate the effects of **RC** and **GC** we also synthesized materials containing only one of these two chromophores (referred to as **PR** and **PG**, respectively). Table 1 summarizes the composition of **PW**, **PR** and **PG**.

OLEDs based on each of the three copolymers (**PW**, **PR**, **PG**) were fabricated by spin-coating the respective material from a toluene solution onto a glass substrate covered with indium-tin-oxide (ITO) and a 35 nm thick layer of PEDOT/PSS (see Experimental). Figure 1 shows typical current-voltage-luminescence characteristics of devices based on an 80 nm thick emissive layer. The devices based on **PW** turn on well

---

[*] Prof. K. Meerholz, M. C. Gather, Dr. R. Alle
Institut für Physikalische Chemie, Universität zu Köln
Luxemburgerstr. 116, 50939 Köln (Germany)
E-mail: klaus.meerholz@uni-koeln.de
Dr. Heinrich Becker
Merck KGaA - Dept. LC/OLED
Industriepark Höchst, Building G865
65926 Frankfurt (Germany)

[**] The authors thank M. Flämmich (Fraunhofer IOF, Jena) for the optical characterization of the white-emitting polymer and Dr. D. Hertel for support with the temperature-resolved measurements. The authors also thank Dr. A. Ludemann for the synthesis of the polymers and Dr. S. Heun (both Merck KGaA) for useful discussion. The authors acknowledge financial support from the Bundesministerium für Bildung und Forschung (BMBF) through the Hobbit project (13N8952).

Table 1. Composition of the white-emitting copolymer PW, the model polymers PG and PR, and electrochemical data for the individual components of the three polymers.

	BB	**HT**	**BC**	**GC**	**RC**
PW feed ratio [mol %]	78.91	10	11	0.05	0.04
PG feed ratio [mol %]	78.95	10	11	0.05	0.00
PR feed ratio [mol %]	78.96	10	11	0.00	0.04
E_{ox} [V] [a]	0.80	0.13	0.38	0.32	0.56
E_{red}, [V] [a]	–	–	–	ca –2.22	–1.64
Band gap [eV] [b]	2.98	–	–	2.48	2.15
$-E_{HOMO}$ [eV] [c]	5.95	5.28	5.53	5.47	5.71
$-E_{LUMO}$ [eV]	2.97 [d]	–	–	2.99 [d] 2.93 [c]	3.56 [d] 3.51 [c]

[a] Measured by cyclic voltametry (CV), values referenced to E_α of ferrocene, $\Delta E_{ox/red} = \pm 10$ meV. [b] Defined by crossing of excitation and emission spectra. [c] Estimated from $E_{ox/red}$, see text for details. [d] Estimated from E_{HOMO} and the optical band gap.

below 3 V, operate at low voltages – 500 cd/m^2 are reached below 5 V – and achieve a peak efficiency of 6.1 cd/A (4 lm/W) at practically relevant brightness levels around 1,000 cd/m^2. At this brightness level the CIE coordinates are (0.338, 0.365) which corresponds to a warm white emission. The CRI is 88, indicating that the spectral composition of the light is well suited for indoor illumination. The devices show high stability, typical half-brightness lifetimes at an initial brightness of 500 cd/m^2 were 1300 h. Compared to devices based on **PW** and **PR** the current density at any given voltage is higher in devices based on **PG**. Since great care was taken to ensure that the layer thickness was identical for all devices this difference indicates a lower conductivity of **PW** and **PR**. As discussed below this is most likely due to the red chromophore acting as an electron trap in OLEDs based on these polymers.

In order to investigate the color-stability of our devices over a wide range of brightness levels, electroluminescence (EL) spectra were recorded at different applied voltages, starting from the onset of detectable luminescence at 2.4 V (corresponding to a brightness of about 0.03 cd/m^2) up to the saturation limit of the spectrometer that was reached at 7.2 V or 6000 cd/m^2. As shown in Figure 2, which displays the series of EL spectra normalized to the shortest-wavelength peak, the emission covers the entire visible spectrum. The EL spectra of devices based on **PG** and **PR** (not shown here) allow assigning the different peaks to the three different chromophores. The peaks at 457 and 485 nm originate from **BC**, the peak at 522 nm corresponds to emission from **GC** and the broad band centered at 610 nm stems from **RC**. While the spectrum is clearly dominated by emission from **RC** at low voltages, the relative contribution of red emission decreases by a factor of 30 compared to the **BC** peak as the voltage is gradually increased. Since the reduction is most pronounced at low voltages the change is less drastic but still clearly visible over the range of practically relevant voltages (3.4-6.4 V) and brightness levels (50–5000 cd/m^2). In contrast to this very strong effect, the relative amount of green emission even slightly increases with voltage (see inset to Fig. 2). As a measure of the relative proportion of emission stemming from **RC** and **GC** we

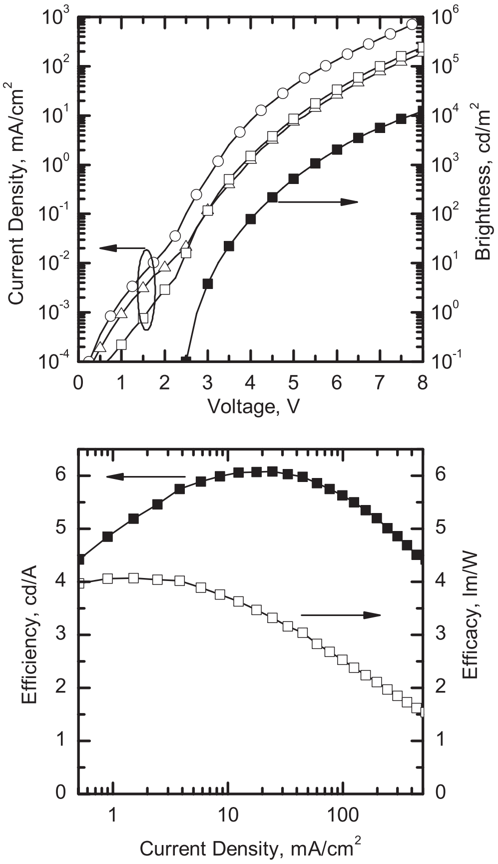

Figure 1. Top, left axis: Current-voltage characteristics of OLEDs based on **PW** (squares), **PR** (triangles), and **PG** (circles). Top, right axis (closed squares): brightness versus applied voltage for the device based on **PW**. Bottom: Current efficiency (closed squares) and power efficiency (open squares) of the device based on **PW**.

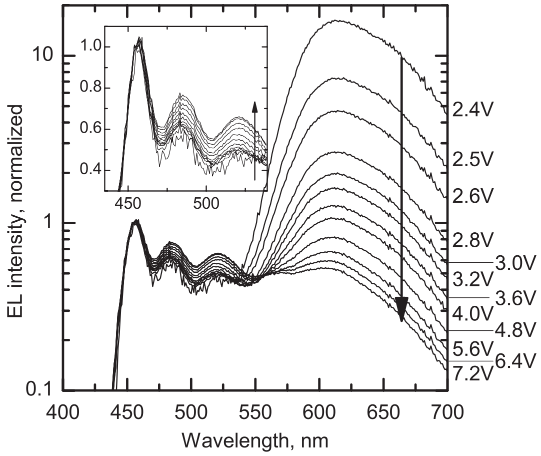

Figure 2. Change of the electroluminescence spectrum of a WOLED based on **PW** with operating voltage. At low voltage the spectrum is entirely dominated by emission from the red-emitting chromophore, whereas the blue emission becomes dominant at higher voltages. The data is displayed on a logarithmic scale to allow comparability of all spectra in one plot. The inset displays the blue and the green peak on a magnified linear scale.

define the ratio $R_{\mathrm{red/blue}}$ and $R_{\mathrm{green/blue}}$ between the peak intensity of the red (610 nm) / green (522 nm) and the blue (457 nm) emission peak. The plot of $R_{\mathrm{red/blue}}$ versus voltage in Figure 3 shows that after an initial dramatic decay $R_{\mathrm{red/blue}}$ converges towards a small non-zero value whereas $R_{\mathrm{green/blue}}$ slightly increases with voltage.

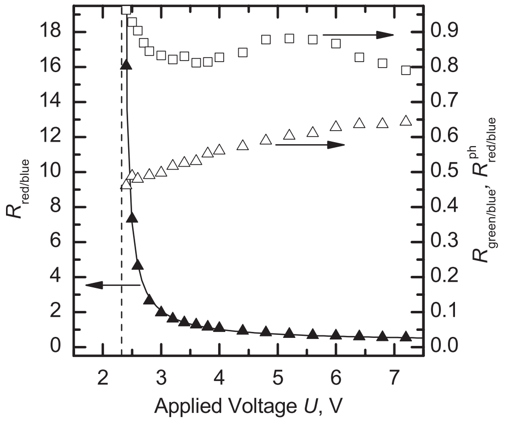

Figure 3. Ratio of the emission intensities at 610 nm and 457 nm ($R_{\mathrm{red/blue}}$, closed triangles) and at 522 nm and 457 nm ($R_{\mathrm{green/blue}}$, open triangles) for a WOLED based on **PW** versus the applied voltage. The figure compares the experimental data to the theoretical expectation for $R_{\mathrm{red/blue}}$ according to Eq. 6 (solid line). The dashed line indicates the estimated built-in voltage U_0. See text for detailed discussion. The open squares show the ratio of red-to-blue emission $R^{\mathrm{ph}}_{\mathrm{red/blue}}$ for a device that was optimized for color stability (**PG** blended with Ir (piq)$_2$ (acac), see text).

Due to the typically very low concentration of the long-wavelength emitting species, saturation of the chromophore has been discussed as a possible cause for the color-shift observed when increasing the brightness of the device.[12] However, we argue that the effect is not relevant here since this would influence the emission from **GC** as well. Furthermore, although the concentration of **RC** is only 0.04 mol % (corresponding to a density of approximately $10^{23}\,\mathrm{m}^{-3}$) the charge carrier density inside the organic layer of the device is expected to be orders of magnitude lower than the chromophore concentration. To give additional experimental evidence for this view the EL spectra of our devices were measured at a constant voltage for a range of temperatures between room temperature and 120 K. As an example, Figure 4 shows spectra recorded at $U = 5$ V. Although the current density decreases dramatically as the temperature is gradually reduced to 120 K (from 10 mA/cm^2 at room temperature to less than 1 μA/cm^2 at 120 K for the case of $U = 5$ V) the shape of the emission spectrum hardly changes, which is very clear evidence that the relative amount of red emission does not depend on the current- or charge-carrier-density in the device. Similar results, i.e. a constant spectrum, were obtained for other voltages.

We also performed optical simulations to investigate whether interference effects can have a significant influence on the spectral composition of the emitted light (see Experimental for details). One possible cause for a change of the emission spectrum would be a shift of the emission zone with increasing brightness, i.e. a variation of the distance between the emission zone and the reflective cathode. Alternatively, the spectral change could be caused by a broadening of the emission zone. Our simulations indicate that the optimum distance for efficient outcoupling of light generated in the organic layer strongly depends on the wavelength. Generally speaking, to achieve more efficient outcoupling of red light, a greater distance between emission zone and cathode is desired than for blue light.[19] As illustrated in Figure 5 a change

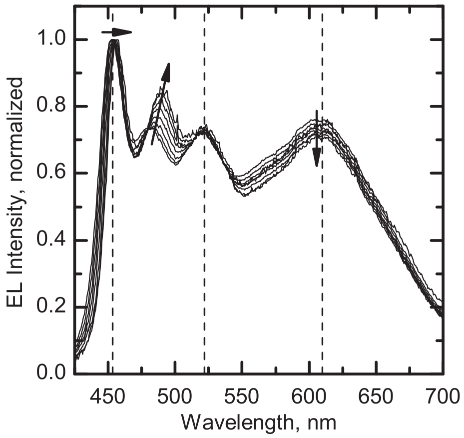

Figure 4. Electroluminescence spectra of a WOLED based on **PW** recorded at a constant voltage (5 V) over a range of temperatures between 295 K and 120 K. The arrows indicate the change of the EL spectrum with decreasing temperature. All spectra are normalized to the short-wavelength peak. Although the current density decreases from 10 mA/cm^2 at 295 K to 1μA/cm^2 at 120 K the ratio of the three main peaks (indicated by dashed lines) changes marginally compared to the effect observed when changing the electric field (see Fig. 2 and 3).

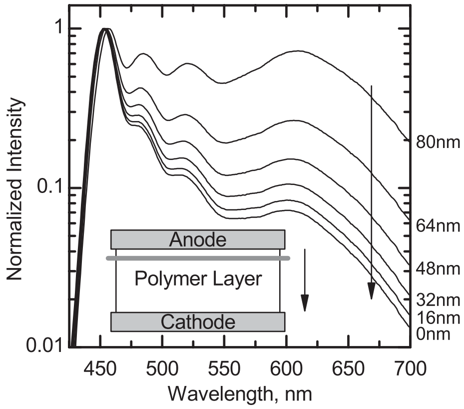

Figure 5. Simulation of the EL spectra from 80 nm thick WOLEDs based on **PW** with infinitely thin emission zones located at six different distances from the reflective metal cathode (80, 64, 48, 32, 16, and 0 nm away from the cathode). The internal emission spectrum was determined from the measured EL spectrum at 5 V using a reverse iteration procedure. As the emission zone moves towards the cathode outcoupling of light with longer wavelength becomes less favorable. The scheme illustrates the shift of the emission zone (indicated by the thick grey line) towards the cathode.

of the red-to-blue emission-ratio by a factor of ten would be expected if the location of the emission zone is shifted from the anode to the cathode interface. Although the simulation illustrates that optical interference effects have a strong influence on the spectral composition of WOLEDs, the effect cannot explain the brightness-dependent color-shift: Our experimental data show that the relative contribution from **GC** even slightly increases with increasing voltage (see inset to Fig. 2). If a shift of the emission zone with increasing brightness were the origin of the color-shift one would expect that (as the refractive index of **PW** is nearly constant over the visible part of the spectrum) the effect of reduced outcoupling efficiency gradually increases towards longer wavelengths. This would imply that the relative amount of green emission would also decay (compare Fig. 5). Since the EL spectrum for a device with a broad emission zone is simply the spectral superposition of several thin emission zones, the above argumentation also applies for a broadening of the emission zone.

From what we have shown so far, neither chromophore saturation nor a brightness-dependent shift or broadening of the emission zone are plausible explanations for the observed color-shift. In the following we discuss if a field-dependent competition between charge trapping and unperturbed charge transport can consistently explain our observations. To identify the components of the polymer which could act as charge trapping centers or charge transport sites, cyclic voltammetry (CV) measurements were performed on model oligomers of **RC** and **GC** (end-capped with mono-functional **BB)**, on a homo-polymer consisting of **BB** alone, and on **PW**. For **RC** and **GC** both the oxidation and the reduction potential are directly accessible via CV. The reduction potential of **BB**, however, is outside the measurement window of the solvent (dichloromethane). Its reduction potential was therefore estimated from the oxidation potential and the optical bandgap (defined as the crossing between the normalized excitation and emission spectra). Once the oxidation potentials of **BB**, **RC** and **GC** are known, the peaks in the CV spectrum of **PW** can be associated with the oxidation potentials of **HT** and **BC**. The oxidation and reduction potentials were converted into HOMO/LUMO energies assuming a constant offset of 5.15 eV. Table 1 summarizes the oxidation and reduction potentials of the different components and lists estimates of the HOMO/LUMO levels.

While the LUMO levels of **GC** and **BB** are almost the same, the LUMO of **RC** is 500-600 meV below **BB** which indicates that **RC** acts as a deep electron trap within the copolymer. However, as we will discuss later, it is not clear whether the concentration of **RC** is sufficiently high to alter the charge transport. Since the LUMO levels of **HT** and **BC** are expected to be well above the LUMO level of the backbone the charge transport is most likely mediated through the high electron-mobility **BB** material. The relatively high HOMO level of **HT** indicates that positive charges will be preferentially localized on these sites and that hole-injection from typical anode materials such as PEDOT:PSS (with a work function around –5.1 eV) is efficient. However, the relatively low concentration of **HT** (10 mol%) is expected to hinder hopping transport between the **HT** sites and thus reduces the mobility of the injected holes.[20, 21] Therefore, we assume that the recombination of electrons and holes in devices based on **PW** occurs predominantly in proximity of the hole-injecting contact.

Based on these assumptions we can develop a model of the competition between electron transport and electron trapping in the thin polymer film. The mobile carrier lifetime τ (i.e. the average time it takes until an electron becomes trapped on an **RC** site) can then be easily estimated: Let N_T be the density and R be the trapping radius of **RC** sites in the polymer film. According to the mean free path approximation, the average distance a charge travels before reaching an **RC** trapping center is given by

$$L_T = \frac{1}{\pi R^2 N_T} \tag{1}$$

As electrons are transported both by drift and by diffusion each of the two mechanisms contributes to charge trapping. Using a simple charge diffusion estimate the diffusion-induced trapping rate $\tau_{\mathrm{Diff}}^{-1}$ is given by

$$\tau_{\mathrm{Diff}}^{-1} = \frac{D}{L_T^2} \tag{2}$$

where D is the diffusion coefficient of the electrons. The drift induced trapping rate $\tau_{\mathrm{Drift}}^{-1}$ depends on the average drift velocity v of the electrons which can be expressed in terms of the electron mobility μ and the electric field $(U - U_0)/d$ dropping across the polymer film with a thickness d:

$$\tau_{\mathrm{Drift}}^{-1} = \frac{v}{L_T} = \frac{\mu}{L_T}\frac{U - U_0}{d} \tag{3}$$

Here U is the voltage applied to the device and U_0 is the built-in field. The overall trapping rate τ^{-1}corresponds to the sum of the drift and the diffusion induced trapping rates:

$$\tau^{-1} = \tau_{\mathrm{Diff}}^{-1} + \tau_{\mathrm{Drift}}^{-1} \tag{4}$$

Once electrons have been trapped on **RC** sites, exciton formation and subsequent radiative relaxation can take place by recombination with holes. Since the depth of the **RC** trapping sites exceed 500 meV, detrapping is unlikely to occur.

We can also give an estimate for the average time τ_{Transit} it takes for a charge to transit through the polymer layer:

$$\tau_{\mathrm{Transit}} = \frac{d^2}{\mu(U - U_0)}\,. \tag{5}$$

The inverse of this time $\tau_{\mathrm{Transit}}^{-1}$ corresponds to the rate at which electrons transit the polymer layer if they are not trapped on an **RC** site. In the vicinity of the anode interface any untrapped electrons will recombine with holes to form excitons that radiatively decay on the **BC** and **GC** sites. Due to good overlap of their emission and absorption spectra, energy transfer from **BB** or **BC** to **GC** is relatively efficient. This explains why there is a significant proportion of green emission although the fraction of **GC** in the polymer is extremely low.

We now consider the ratio of the trapping rate $\tau^{-1}$and the transit rate $\tau_{\mathrm{Transit}}^{-1}$:

$$q(U) = \frac{\tau^{-1}}{\tau_{\mathrm{Transit}}^{-1}} = \frac{D}{\mu}\left(\frac{d}{L_T}\right)^2 \frac{1}{U - U_0} + \frac{d}{L_T} \qquad (6)$$

This quantity provides an estimate of the proportion of charges that are trapped on the red-emitting chromophore (and eventually generate red emission) and those which cross the polymer film untrapped (and eventually generate blue and green emission). It is therefore expected that $q(U)$ is proportional to the ratio between the red and the blue emission (i.e. to the quantity $R_{\mathrm{red/blue}}$ defined above) and that the voltage dependence of $q(U)$, which originates from trapping induced by charge diffusion (cf. Eq. 2), describes the relative decay of red emission with increasing voltage. The constant offset results from field induced trapping (cf. Eq. 3). The line in Figure 3 represents a least squares fit of $q(U)$ to the experimental data ($R_{\mathrm{red/blue}}$). The excellent fit (correlation coefficient $R^2 = 0.999$) is a very strong indication that - despite being quite simple - our model is adequate to explain the origin of the observed color-shift. The good fit also confirms that the above assumptions are justified and that detrapping effects are not relevant. Our approach allows a precise measurement of the built-in voltage U_0 of our devices. We obtain $U_0 = 2.32$ V which is in very good agreement with the threshold for current injection. Furthermore, the obtained fit parameters indicate that the Einstein relation (D/μ = 25 meV) is not valid for **PW**, since this would result in a mean free path length L_D of 0.5 nm. If we assume $L_D = 100$ nm (which is consistent with our picture of partial charge trapping on **RC**) we obtain at a D/μ ratio of 5.3 eV. We note that the D/μ ratio in organic semiconductors does not necessarily agree with the Einstein relation and that significant deviations have been reported in the literature for various materials.[22,23]

To prevent the field-dependent color-shifts and to provide further evidence for the model developed here we replaced **RC** by a red-emitting chromophore that does not constitute an electron trap. In this case the major excitation-route for the chromophore is energy transfer that is not influenced by the applied field. The choice of suitable red-emitting chromophores is difficult due to their intrinsically low bandgap. One way to overcome this problem is by using a red-emitting phosphorescent dye. Due to the triplet-singlet exchange energy, the HOMO/LUMO gap of such a dye is larger than for a fluorescent chromophore emitting at the same wavelength. As one possible example of such a dye we blended the iridium complex $\mathrm{Ir(piq)_2(acac)}$ (purchased from American Dye Sources) with the copolymer **PG** that does not contain **RC**. We previously measured the HOMO/LUMO energies of $\mathrm{Ir(piq)_2(acac)}$ to $E_{\mathrm{HOMO}} = -5.46$ eV and $E_{\mathrm{LUMO}} \geq -2.40$ eV.[24] These values indicate that the complex is not a trap for either electrons or holes in our case. A device containing an 80 nm thick layer of **PG** blended with 1 wt% of $\mathrm{Ir(piq)_2(acac)}$ emits a balanced white EL spectrum that remains stable over the entire measurement range (2.4 V – 7.2 V). The open squares in Fig. 3 correspond to the red-to-blue ratio of this device. Compared to the results obtained for **PW** the relative contribution of the red emission is hardly affected by the applied voltage and is now similar to the shift of the emission from **GC**. Furthermore, the voltage required for any given current density is not increased by the addition of $\mathrm{Ir(piq)_2(acac)}$, again indicating that the dye is not a trap for electrons. The efficiency of these devices is considerably lower (2.7 cd/A) than for the **PW** based devices (6.1 cd/A). We point out that the phosphorescent dye doped OLEDs were not yet optimized for efficiency but were fabricated to proof that the color-stability can be greatly enhanced if electron trapping is avoided. Systematic material and device optimization will be required in order to increase the device efficiency and to avoid losses that could be associated with back transfer of triplet states from the red-emitting chromophore to the host.

In conclusion, we have shown that the color-shift observed in WOLEDs based on a single emissive layer of a white-emitting copolymer originates from the competition between electron trapping on red-emitting sites and unperturbed charge transport through the organic layer. Since the trapping rate of electrons depends on the electric field inside the emissive layer the proportion of red emission is related to the applied field rather than to the current density. Due to the inherently low bandgap of red-emitting chromophores it seems likely that the field-dependent charge trapping mechanism plays a major role in many single layer WOLED structures reported in the literature. In multilayer based WOLEDs, however, the situation is more complicated, since one has to take the field dependence of hole and electron transfer rates across each interface into account. The color-shift was suppressed by employing a phosphorescent red-emitting chromophore that does not constitute an electron trap. Other approaches for improving the color-stability could include the use of multilayer structures in which the low-bandgap electron trapping material is separated from the electron transporting layer.

Experimental

Synthesis: The general synthesis of the electroluminescent polymers has been described elsewhere [25-27].

OLED Fabrication: Indium-tin-oxide (ITO) coated soda-lime glass substrates (Merck, Darmstadt) were thoroughly cleaned and exposed to ozone treatment for 10 min. A 35 nm thick layer of PEDOT:PSS (Baytron P AI4083) was spin-coated onto the substrates under cleanroom conditions and heated to 110 °C for 1 min to remove residual water. After transfer of the substrates to a nitrogen glovebox an 80 nm thick layer of **PW**, **PG** or **PR** was spin-coated from a toluene solution (10 g/l) and cured at 180 °C for 10 min. To fabricate the devices with improved color-stability, the iridium complex $\mathrm{Ir(piq)_2(acac)}$, which was purchased from American Dye Sources, was dissolved in toluene and mixed with the **PG** solution prior to spin-coating. The substrates were transferred to a high-vacuum chamber for evaporation of the cathode (consisting of 4 nm barium covered by 150 nm silver). All devices were encapsulated with a glass cover plate to allow for extensive characterization outside the glove-box.

Characterization: Current-voltage-luminance characteristics were measured with a Keithley 2400 source meter and a calibrated photodiode. The EL spectra were recorded with a fluorescence spectrometer (Cary Eclipse, Varian) equipped with a highly sensitive photo-multiplier detector. For the temperature dependent measurements a CryoVac Continuous Flow cryostat system and a Roper Scientific PI-MAX2 camera attached to an Acton Spectra Pro 2300i monochromator were used.

Cyclic Voltammetry: Voltammagrams were recorded with an EG+G Instruments Potentiostat/Galvanostat M283. The measurements were performed in CH_2Cl_2 with $TBAPF_6$ (0.1 M) as the supporting electrolyte. Disk shaped platinum ($A = 0.2\,mm^2$) was used as working electrode, a platinum wire as counter electrode and a silver wire as reference electrode. All potentials cited are given vs. the potential of the ferrocene/ferrocenium redox couple.

Optical Simulations: All simulations were performed with ETFOS (Vers. 1.3), which relies on computing the far field distribution of emissive dipoles in the emissive layer to calculate the EL spectrum. The **PW** dipole emission spectrum was determined from the measured EL spectrum (taken at 5 V) using a reverse iteration procedure (assuming that the emission zone is located at the anode interface). The dispersive complex refractive indices of all layers in the OLED stack were calculated from transmission and reflection spectra [28] of thin films of the respective materials.

Received: July 10, 2007
Revised: August 2, 2007

[1] B. W. D'Andrade, S. R. Forrest, *Adv Mater* **2004**, *16*, 1585.
[2] A. Misra, P. Kumar, M. N. Kamalasanan, S. Chandra, *Semicond. Sci. Technol.* **2006**, *21*, R35.
[3] Y. R. Sun, N. C. Giebink, H. Kanno, B. W. Ma, M. E. Thompson, S. R. Forrest, *Nature* **2006**, *440*, 908.
[4] X. Gong, S. Wang, D. Moses, G. C. Bazan, A. J. Heeger, *Adv. Mater.* **2005**, *17*, 2053.
[5] Y. Duan, W. L. Jiang, J. Li, G. Chen, Y. Zhao, J. Y. Hou, S. Y. Liu, *Jpn. J. Appl. Phys. Part 1* **2004**, *43*, 7501.
[6] S. K. Kwon, Y. K. Lee, T. J. Park, H. Uchiike, J. H. Kwon, J. Jang, J. K. Jin, D. C. Shin, H. You, *Mol. Cryst. Liq. Cryst.* **2006**, *458*, 263.
[7] C. Serwatzy (AEG; MIS, Ulm), personal communication.
[8] M. Berggren, O. Inganas, G. Gustafsson, J. Rasmusson, M. R. Andersson, T. Hjertberg, O. Wennerstrom, *Nature* **1994**, *372*, 444.
[9] C. H. Kim, J. Shinar, *Appl. Phys. Lett.* **2002**, *80*, 2201.
[10] H. A. Al Attar, A. P. Monkman, M. Tavasli, S. Bettington, M. R. Bryce, *Appl. Phys. Lett.* **2005**, *86*, 121101.
[11] J. Liu, Z. Y. Xie, Y. X. Cheng, Y. H. Geng, L. X. Wang, X. B. Jing, F. S. Wang, *Adv. Mater.* **2007**, *19*, 531.
[12] B. Hu, F. E. Karasz, *J. Appl. Phys.* **2003**, *93*, 1995.
[13] P. I. Shih, Y. H. Tseng, F. I. Wu, A. K. Dixit, C. F. Shu, *Adv. Funct. Mater.* **2006**, *16*, 1582.
[14] J. H. Park, T. W. Lee, Y. C. Kim, O. O. Park, J. K. Kim, *Chem. Phys. Lett.* **2005**, *403*, 293.
[15] J. Liu, Q. Zhou, Y. Cheng, Y. Geng, L. Wang, D. Ma, X. Jing, F. Wang, *Adv. Mater.* **2005**, *17*, 2974.
[16] A. Falcou, A. Büsing, S. Heun, J. Steiger, A. Gerhard, N. Schulte, H. Becker, *WO Patent 05/030827*.
[17] D. Buchhauser, C. Heuser, A. Hunze, H. Becker, A. Büsing, A. Falcou, L. Rau, S. Vögele, S. Göttling, *Proc. SPIE-Int. Soc. Opt. Eng.* **2004**, *5219*, 70.
[18] S. Bange, A. Kuksov, D. Neher, "Revealing the Dynamics in Polymer-based Optoelectronic Devices", *Symposium Organic Thin Film Electronics: From Molecular Contacts to Devices (SYOE)* DGG Frühjahrstagung **2007**.
[19] M. C. Gather, K. Meerholz, unpublished.
[20] F. Laquai, G. Wegner, C. Im, H. Bässler, S. Heun, *J. Appl. Phys.* **2006**, *99*, 023712.
[21] F. Laquai, D. Hertel, *Appl. Phys. Lett.* **2007**, *90*, 142109.
[22] M. C. Gather, S. Mansurova, K. Meerholz, *Phys. Rev. B* **2007**, *75*, 165203.
[23] A. Hirao, H. Nishizawa, M. Sugiuchi, *Phys. Rev. Lett.* **1995**, *75*, 1787.
[24] X. H. Yang, D. C. Müller, D. Neher, K. Meerholz, *Adv. Mater.* **2006**, *18*, 948.
[25] C. D. Müller, A. Falcou, N. Reckefuss, M. Rojahn, V. Wiederhirn, P. Rudati, H. Frohne, O. Nuyken, H. Becker, K. Meerholz, *Nature* **2003**, *421*, 829.
[26] H. Becker, E. Breuning, A. Falcou, S. Heun, A. Parham, H. Spreitzer, P. Stößel, J. Steiger, *Proc. Mat. Res. Soc.* **2003**, *769*, 3.
[27] H. Becker, K. Treacher, H. Spreitzer, A. Falcou, A. Büsing, A. Parham, *WO Patent 03/020790*.
[28] J. M. Delpozo, L. Diaz, *Appl Optics* **1992**, *31*, 4474.